Pergamon

Int. J. Heat Mass Transfer. Vol. 40, No. 6, pp. 1467–1480, 1997

0017-9310/97 $17.00+0.00

PII: S0017-9310(96)00167-6

Flow structure and temperature measurements in a 3-D vertical free convective enclosure at high Rayleigh numbers

SHOU-SHING HSIEH and SHYH-SHYAN YANG

Department of Mechanical Engineering, National Sun Yat-Sen University, Kaohsiung, Taiwan 80424, Republic of China

(*Received* 15 *February* 1996 *and in final form* 23 *April* 1996)

Abstract—Experimental studies were performed and boundary-driven flows in a differentially heated water and silicone oil filled rectangular enclosure with aspect ratios H/L of 20 and $W/L = 6$ at high Rayleigh number range 1.58×10^8–1.48×10^{10}. Flow visualization was made and velocity profiles were obtained using a two component laser-Doppler velocimeter for different Rayleigh numbers. The vertical and horizontal temperature distributions in the core were measured and compared with previous related studies. Furthermore, thermal correlations as a function of Rayleigh numbers and geometrical parameters and working fluids for different regimes were developed, which were also verified by relevant existing results. Copyright © 1996 Elsevier Science Ltd.

1. INTRODUCTION

Buoyancy-driven fluid flows in enclosures with differentially heated vertical walls have been a topic of long-term interest because of their applications in a number of areas, such as heating and cooling of buildings, cryogenic storage tanks, the cooling of electronic components and solar energy collectors and because of their fundamental importance, such as the complexity of the internal recirculating flows. Extensive reviews of the work were given by Ostrach [1, 2] and Bejan [3].

The major dimensionless parameters that determine the structure of a constant property flow in a differentially heated enclosure are the Rayleigh number,

$$Ra = g\beta(T_H - T_C)H^3/\alpha\nu$$

the Prandtl number

$$Pr = \nu/\alpha$$

and the enclosure vertical and horizontal aspect ratios ($A_H = H/L$ and $A_W = W/L$). A good description of the influence of Ra and Pr in determining the flow regimes has been given by Hiller *et al.* [4]. Moreover, the geometry of the enclosure was also found to be significant in determining the flow regimes (see, for example, Hoogendoorn [5]).

Although there have been a number of analytical, numerical, and experimental studies for low to moderate values of Rayleigh numbers that comprise laminar flows (see, for example, Ozoe *et al.* [6]), far fewer studies have been reported for high Rayleigh number transitional and turbulent flows. Recently, Lankhorst *et al.* [7] studied experimentally buoyancy-induced flows with differentially heated vertical walls in an enclosure at the high Rayleigh number range of 1.0×10^9–4.0×10^9. LDV measurements were carried out for the vertical velocity component. The data can form a basis for numerical modeling of transitional and turbulent buoyancy driven convection in enclosures.

In spite of this, it is found that, experimental data in the range of $Ra \approx 10^{10}$ are scarce. It is essentially necessary to experimentally understand the form or significance of the buoyance-induced flows in a rectangular enclosure at high Rayleigh numbers. The present paper is a continuation of work by Hsieh and Wang [8] for 3-D natural convection in enclosures with different working fluids at Rayleigh numbers of 8.7×10^2–2.0×10^9.

The primary objective of this study is to present more complete experimental velocity LDV measurements including horizontal velocity components. Also the range of Ra will be extended to 1.48×10^{10} to broaden our fundamental understanding of the flow characteristic in this type of buoyancy-induced flow in a rectangular enclosure. Moreover, since 3-D measurements are quite scarce, the data obtained herein should be useful in 3-D numerical code validation and the assessment of the assumption of two-dimensionality in previous experiments with high aspect ratios and high Rayleigh numbers, especially at $Ra \cong 1.5 \times 10^{10}$.

In this paper, results were presented for 3-D flow fields using both a laser-Doppler velocimeter and flow visualization and for the corresponding temperature measurements using a thermocouple in a rectangular enclosure with two differentially heated vertical walls, as shown in Fig. 1.

NOMENCLATURE

A	area of wall [m^2]
A_H	vertical aspect ratio H/L
A_W	horizontal aspect ratio W/L
g	acceleration due to gravity [m s^{-2}]
Gr	Grashof number $g\beta(T_H-T_C)H^3/\nu^2$
H	height of slot [m]
h	heat transfer coefficient [W m^{-2} K^{-1}]
k	thermal conductivity [W m^{-1} K^{-1}]
L	width of slot [m]
Nu	Nusselt number
Pr	Prandtl number ν/α
Q	heat transfer rate [W]
Ra	Rayleigh number $g\beta(T_H-T_C)H^3/\nu\alpha$
T	temperature [K]
u	x component velocity [cm s^{-1}]
v	y component velocity [cm s^{-1}]
w	z component velocity [cm s^{-1}]
W	length of slot [m]
x	direction parallel to the width of the slot
y	direction parallel to the height of the slot
z	direction parallel to the length of the slot
u^+	dimensionless x component velocity u/u_{max}
v^+	dimensionless y component velocity v/v_{max}
w^+	dimensionless z component velocity w/w_{max}
x^+	dimensionless width x/L
y^+	dimensionless height y/H
z^+	dimensionless length z/W.

Greek symbols

α	thermal diffusivity of fluid [m^2 s^{-1}]
β	thermal expansion coefficient [K^{-1}]
θ	dimensionless temperature $(T-T_C)/(T_H-T_C)$
ν	kinematic viscosity of fluid [m^2 s^{-1}].

Subscripts

C	cold wall
H	hot wall
m	reference mean bulk temperature $(T_H+T_C)/2$
max	maximum velocity.

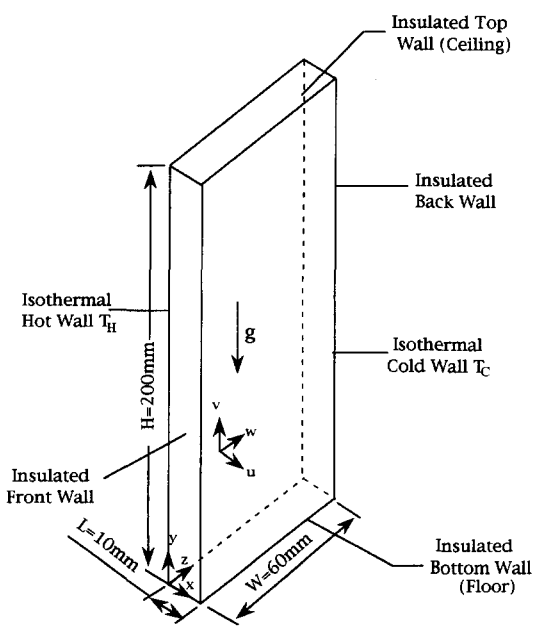

Fig. 1. Schematic of physical and coordinate system.

2. EXPERIMENTAL SET-UP AND PROCEDURE

2.1. *Experimental facility and heat transfer measurements*

The thermal convection flow was generated in a $200\times10\times60$ mm rectangular enclosure. Figure 2 shows the enclosure and the coordinate system used—the y-direction is vertically upwards. The two opposite lateral walls of the box ($x=0$ and $x=L$) were made of copper (5 mm thick) and kept at prescribed constant temperature by two isothermal baths. The other four walls, made from 10 mm plexiglass with 10 mm polystyrene foam, were considered to be thermal insulators when temperature measurements were conducted.

The great thermal capacity and thermal conductivity of the copper walls allowed us to maintain constant and uniform temperatures of the heated and cooled walls. These temperatures were continuously measured by means of copper–constantan thermocouples (AWG 28) and recorded by an OMEGA μR100 automatic data acquisition system. The observed temperature fluctuations were less than 0.2°C.

Heating and cooling of the vertical isothermal walls was accomplished by pumping hot demineralized water at temperature T_H and cold demineralized water at temperature T_C through the double-paned walls. The water was circulated and regulated through commercially available constant temperature baths. Suitable values of T_H and T_C were chosen to minimize the temperature difference between the mean enclosure temperature and the ambient temperature. The temperature differences between the heated and cooled walls was varied in the range of 5–65°C. The ambient temperature was kept at 25°C. The enclosure was filled

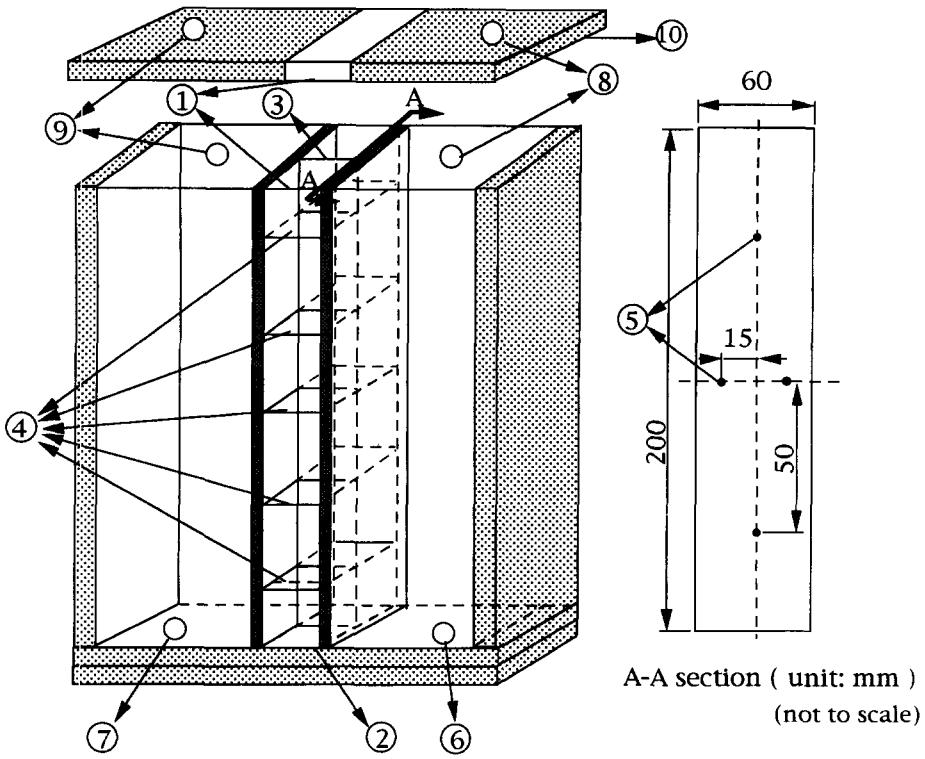

(1) test section
(2) 10mm plexiglass
(3) the vertical(xy) plane at z=0.5W
(4) the horizontal(xz) plane y=0.9H,0.7H ,0.5H,0.3H and 0.1H
(5) wall temperature measurement position(at two opposite vertical walls)
(6) hot water inlet
(7) cold water inlet
(8) hot water outlet
(9) cold water outlet
(10) top ceiling of the enclosure

10mm thickness polystyrene foam thermal insulator

5mm thickness copper plate

Fig. 2. Schematic of test section.

with water and silicone oil, as working fluids for each experimental run.

Five copper–constantan thermocouples were installed at various locations on each of two (heated/cooled) vertical walls. The maximum temperature deviation from the mean temperature of the wall was $\pm 0.1°C$. Wall temperature measurements were taken and averaged arithmetically to obtain T_H and T_C at each steady state. From these $\Delta T(T_H - T_C)$ values required to calculate the Rayleigh and Nusselt numbers were obtained.

The ambient temperature was constantly monitored. The accuracy of all thermocouple measurements was $\pm 0.1°C$. Thermal conditions were stable to within $\pm 0.1°C$ over the measurement period. A very thin (AWG 40) thermocouple probe was inserted through a slot in the top ceiling of the enclosure, approximately in the middle of the vertical sides, and traversed in the horizontal or vertical direction to measure the local temperature of the core. This probe was carefully shifted or lowered to a desired position or depth and held there for 5 min to assure that any flow disturbance had died away. Temperature measurements were thus taken, and the probe was shifted or lowered further until eventually the left vertical wall or bottom wall was reached.

2.2. *Flow visualization*

Flow structures were visualized using photographic records of the motion of tracer particles illuminated by a sheet of white light. Aluminum powders were used as tracer particles. The typical size of the particles was 5–15 μm and their concentration in the working fluid was kept below 0.1% by weight. Time-exposure

(25–30s) photographs were taken of the flow patterns using a Cannon-AE1 camera with Fuji black-and-white ISO 100 films.

2.3. *LDV measurements*

The present system is a commercial two color, four beam DANTEC fringe-type LDV system, operated in the backward scatter mode, with a general layout as shown in Fig. 3. The relevant optical system parameters are listed in Table 1.

Standard DANTEC 55× modular optics and a model Stabilite 2016 4W spectral physics Ar^+ laser are mounted on a 2-D, traversing system. Two separate LDV channels are formed by use of color separation, using 514.5 nm (green light) and 488.0 nm (blue light) wavelength beams. These two beams form orthogonal fringes by means of a standard DANTEC two channels optical train. These two sets of fringes allow the simultaneous measurement of two orthogonal components.

The spanwise velocity component is measured using the 488.0 nm beam, while the 514.5 nm beam measures the streamwise velocity component. A combined counter-type signal processor (Dantec model 57H00), with functions of counter, buffer interface and coincidence filter which is interfaced with a LEO(Intel-486) P.C. in the direct access mode, was employed for data processing. At each measurement location, 3000 measurements were made of the velocity component, from which the time-average was determined and each measurement took 10^{-2} s.

For the present system, the link consisted of four fiber manipulators and four single mode fibers. Each fiber manipulator was used as a launch unit to couple the beam onto the fiber. The single mode polarization preserving fiber produced a beam diameter of 1.35 mm, and beam divergence angle of 0.5–0.6 mrad. It was fitted with two plugs at each end, which included the microlens for focusing (at the receiving end) and/or resetting the divergence angle of the beam (at the probe end). The overall system allowed a coupling efficiency of $\cong 70\%$ to be achieved for laser–fiber coupling.

Table 1. Laser-Doppler velocimeter optical parameter

Parameter	Value
Laser power	4 W
Laser wavelength	
green beam	514.5 nm
blue beam	488.0 nm
Beam-diameter at e^{-2}	
(major and minor axes of ellipsoid)	
green	3.98 mm × 0.189 mm
blue	3.98 mm × 0.189 mm
Beam half angle	
green	6.76°
blue	6.76°
Focal length	
green	160 mm
blue	160 mm
Fringe opening	
green	2.12 μm
blue	2.12 μm
Number of fringes	36

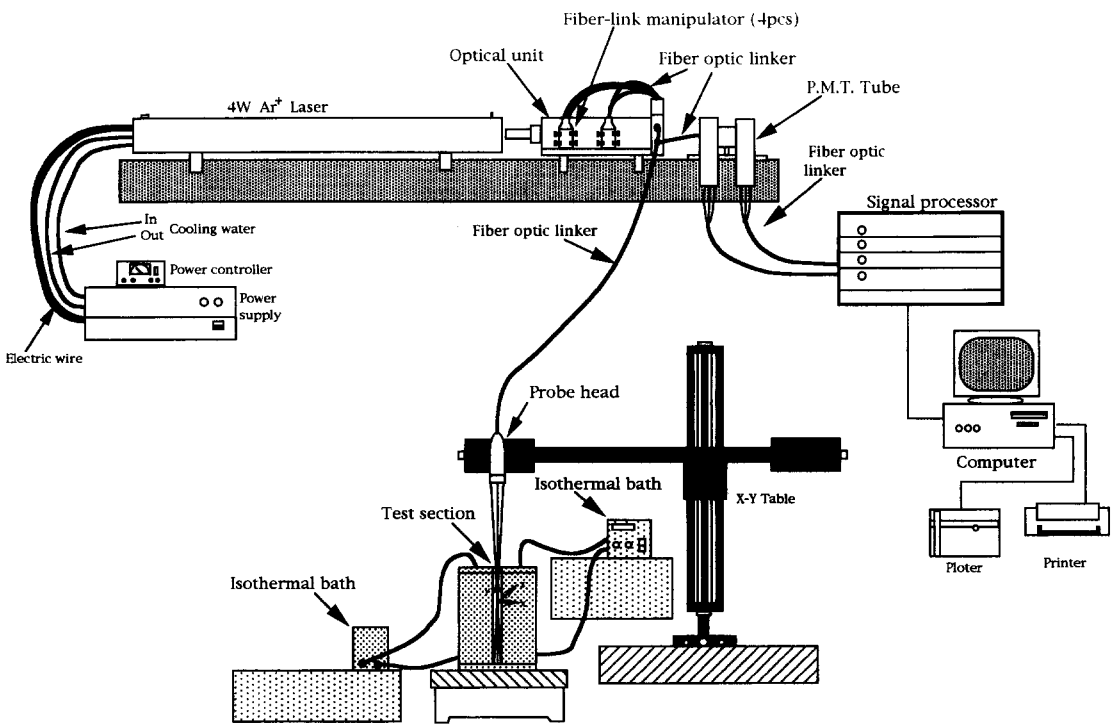

Fig. 3. Experimental setup and LDV measurement details (side view).

3. DATA REDUCTION AND UNCERTAINTY

The average values of the thermophysical properties of the working fluid in the enclosure were obtained at a reference temperature, referred to as a mean bulk temperature of

$$T_m = 0.5(T_H + T_C).$$

The length scale used in calculating the Nusselt number and Rayleigh number is $H = 200 \pm 0.5\%$ mm. The temperature difference used in deriving the Rayleigh number is the difference in temperature between the hot and cold walls, i.e. the overall temperature difference.

The major dimensionless parameters that determine the structure of a constant property flow in a differentially heated enclosure are the Rayleigh number,

$$Ra = g\beta \Delta T H^3 / \nu\alpha \quad (1)$$

and the Prandtl number. The temperature difference used to calculate the heat transfer coefficient is the difference between the two side-wall temperatures

$$Nu = hH/k \quad \text{and} \quad h = Q/A\,|T_H - T_C|. \quad (2)$$

A indicates the area used to derive the heat transfer coefficient which is $120 \pm 1.8\%$ cm^2 for the present study.

For each run, it took about 2–4 h to obtain a steady state. A steady state is indicated by a steady temperature difference (for constant flow rate) in the heating and cooling water for each wall.

The cooling and heating water flow rate, nominally 680 kg h^{-1}, is measured with a rotameter. These were calibrated by the stop watch-and-bucket method to within $\pm 3\%$ for near ambient temperatures for the highest temperatures at which the walls were operated, about 65°C, the flow meter tended to read high by about 3–5% due to a decrease of approximately 2% in the fluid density. Partially offsetting those two uncertainties is an error that increases by about 3% at 25°C owing to nonlinearity of the temperature difference measuring period. Data were corrected for conduction through the neoprene gasket from a heated wall to a cooled wall (about 5%), and for radiation heat transfer from the hot wall to the cold wall (about 2%).

The overall heat balance in the test section (total measured heat transfer from the hot wall minus total measured heat transfer to the cold wall divided by the total measured heat transfer from the hot wall) is typically between $\pm 3\%$ (for the highest Rayleigh number) to $\pm 5\%$ (for the lowest Rayleigh number) and the insulated wall heat loss is about $\pm 5\%$. In spite of this, the overall heat transfer measurements are expected to be within $\pm 10\%$ of the actual convection heat transfer from each wall and ΔT is within the ranges from $\pm 8\%$ (for the highest Rayleigh number) to $\pm 6\%$ (for the lower Rayleigh number).

Based on the afore-mentioned relevant uncertainties, the maximum estimated uncertainties in Ra and Nu are 6–8% and 7–9%, respectively, using the uncertainties estimated procedure described by Kline and McClintock [9]. The uncertainty in the measurement of Doppler frequency is $\pm 0.4\%$. The error in the measurement of velocity is assessed as 1% for all three velocity components. Table 2 lists the range of the properties for silicone and water used in this study and the present maximum variation from average values used in computing the Rayleigh numbers.

4. RESULTS AND DISCUSSION

4.1. *Flow visualization*

To ensure equilibrium conditions the enclosure was left to stabilize for several hours after the aluminum powder had been introduced. The photographs were taken after a steady state had been reached both thermally and hydrodynamically.

In the beginning, interest was directed at understanding the flow in the center of the vertical plane of the enclosure. For this purpose observations of flow patterns were performed for a number of cases with increasing Rayleigh numbers (from 1.58×10^8 to 1.48×10^{10}) for both water and silicone oil.

Figures 4 and 5 show the vertical flow structure of these results. The effect of convection is clearly noted. Particles near the side walls closely follow the form of the enclosure. The patterns show a single cell structure. The cell appears to extend to very near the top or bottom of the enclosure. Strong end effects are shown due to large heat losses from the plexiglass walls, which were not insulated when conducting the flow visualization. Away from the ends, the flow is mainly vertical, with a slight periodic variation in the amplitudes of the vertical velocity.

The waviness at the heated wall, especially for Fig. 4, due to the lower viscosity of water was also observed by the naked eye. The waves appear to break near the top or bottom of the enclosure. The waviness in the boundary layer occurred at the level of local Rayleigh numbers Ra_y estimated to be 1.25×10^9, which coincides with those reported by Elder [10] and Hsieh and Wang [8]. They give the conditions for the onset of boundary layer waves as $Ra_y = 3 \times 10^8$ and $Ra_y = 6 \times 10^8$, respectively, for $H/L \cong 10$.

The lack of symmetry in the enclosure is mainly attributed to fluid property variations with temperature; it may also be due to different heat loss through the top and bottom walls. Bergholz [11] has estimated that for water when A_H is greater than 97, multicellular motion convection can take place; below this value the instability is of a traveling-wave type. Lee and Korpela [12] showed that there is no trace of traveling waves for $A_H = 10$ and 15 when $Ra \cong 4 \times 10^5$.

Based on these two previous studies and the present visualization, one can conclude that the traveling-wave instability can be found for water. This traveling wave speed was much slower than the convection flow velocity. The waves found represent transition of the

Table 2. Physical properties of silicone oil and water used

Temperature [K]	Viscosity [$m^2 s^{-1}$]	Thermal conductivity [$W m^{-1} K^{-1}$]	Thermal diffusivity [$m^2 s^{-1}$]	Specific heat [$kJ kg^{-1} K^{-1}$]	Prandtl number	Maximum variation of the viscosity
298	50×10^{-6}	0.154	1.06×10^{-7}	1.52	472	$\pm 4.2\%$
	(0.89×10^{-6})	(0.6)	(1.44×10^{-7})	(4.179)	(8.4)	$(\pm 4.1\%)$
303	47.9×10^{-6}	0.1538	1.05×10^{-7}	1.532	457	$\pm 4.0\%$
	(0.8×10^{-6})	(0.61)	(1.46×10^{-7})	(4.178)	(5.5)	$(\pm 4.1\%)$
308	45.8×10^{-6}	0.153	1.03×10^{-7}	1.544	444	$\pm 3.8\%$
	(0.72×10^{-6})	(0.62)	(1.49×10^{-7})	(4.178)	(4.8)	$(\pm 3.9\%)$
313	43.7×10^{-6}	0.1529	1.02×10^{-7}	1.556	427	$\pm 3.9\%$
	(0.66×10^{-6})	(0.63)	(1.52×10^{-7})	(4.178)	(4.3)	$(\pm 3.8\%)$
318	41.5×10^{-6}	0.1524	1.01×10^{-7}	1.568	410	$\pm 3.7\%$
	(0.6×10^{-6})	(0.635)	(1.53×10^{-7})	(4.175)	(3.9)	$(\pm 3.8\%)$
323	39.4×10^{-6}	0.1519	1×10^{-7}	1.58	394	$\pm 3.7\%$
	(0.55×10^{-6})	(0.64)	(1.55×10^{-7})	(4.18)	(3.5)	$(\pm 3.9\%)$
328	37.3×10^{-6}	0.1514	0.99×10^{-7}	1.592	377	$\pm 3.8\%$
	(0.51×10^{-6})	(0.645)	(1.56×10^{-7})	(4.182)	(3.3)	$(\pm 3.7\%)$
333	35.2×10^{-6}	0.151	0.98×10^{-7}	1.604	345	$\pm 3.7\%$
	(0.47×10^{-6})	(0.65)	(1.58×10^{-7})	(4.184)	(3.0)	$(\pm 3.7\%)$
338	33×10^{-6}	0.1505	0.97×10^{-7}	1.616	340	$\pm 3.6\%$
	(0.44×10^{-6})	(0.655)	(1.59×10^{-7})	(4.186)	(2.7)	$(\pm 3.8\%)$

( ): stands for property of water.

hot wall boundary-layer. They appear to be of a well organized, single wave length and are essentially 2-D in nature by observation; namely, there seems to be no variations in the depth direction. For silicone oil, as stated in Lee and Korpela [12] for fluids whose Prandtl number is larger than 12.7, the instability can only be observed in very tall cavities (e.g. one which is a hundred times taller than its width).

A general feature common to all the photographs is the entrainment of the flow in the vertical boundary-layers. Notice that the cold wall mass is ejected from the left vertical boundary-layer into the region adjacent to the horizontal surface. The horizontal layer converges toward the lower corner of the hot wall and is then swept up into the right vertical boundary-layer. Similar features are supposedly observed at the upper half of the hot wall, illustrating the odd symmetry pointed out by Morrison and Tran [13] and also shown in the following section for velocity measurements.

The entrainment or detrainment induces a horizontal cross flow in the core region and leads to a vertical temperature gradient in the core. Again, the lack of symmetry in the flow is attributed to the variation of the viscosity with temperature and different heat loss through the top and bottom walls.

The flow in the narrow enclosure remains a single cell up to $Ra = 1.48 \times 10^{10}$. The weak secondary flow (traveling-wave type) appears at $Ra = 4.75 \times 10^9$ in Fig. 4, but it is not observed in Fig. 5. The motion in these traveling-waves intensifies with increasing Ra and, finally, appears to become turbulent at $Ra = 1.48 \times 10^{10}$. Within the boundary-layer regime, where $Ra \leqslant 4.75 \times 10^9$, the layers adjacent to the vertical walls are thinner than those along horizontal walls. The very slow motion that occurs in the core is evident from the ejected particles which are almost stationary. Moreover, the effect of the working fluid as well as Ra on the flow pattern is clearly noted due to the different flow pattern found in Figs. 4–5.

4.2. *Flow structure*

The vertical velocity (v) profile was measured at the vertical central plane of the enclosure for a series of elevations between the bottom of the enclosure and the top end of the wall, see Fig. 6(a). These results indicate that the vertical flow is not uniform over the central segment of the enclosure $0.1H < y < 0.9H$. This is due to boundary-layers growing in the vertical walls. Thus the end wall (top/bottom) affects the flow for a distance considerably greater than that usually shown in 2-D enclosures. The surprising characteristic of these measurements is that the profiles are not symmetric about the midplane, $x^+ = 0.5$. The velocity at $z = 0.5W$ and $y = 0.5H$ near the cold wall is about 15% less than the velocity at a corresponding point near the hot wall.

There are significant differences between the profiles of Morrison and Tran [13] and the present study. Morrison and Tran [13] show a continuous decrease in velocity from the heated wall to the cooled wall; the present results show a flat region of near zero velocity in the center of the enclosure. This is perhaps due to higher levels of mixing in the present case, which is expected since the present flow is turbulent, while Morrison and Tran's flow is at a much lower Ra. Also, a vertical symmetry is not found which was reported by Morrison and Tran [13]. This strongly indicates that the flow structure above/below the horizontal central plane ($y = 0.5H$) is different.

At the region of $0.25 < x^+ < 0.75$, for $y = 0.5H$, $v \cong 0$ indicates that there is no vertical velocity. This

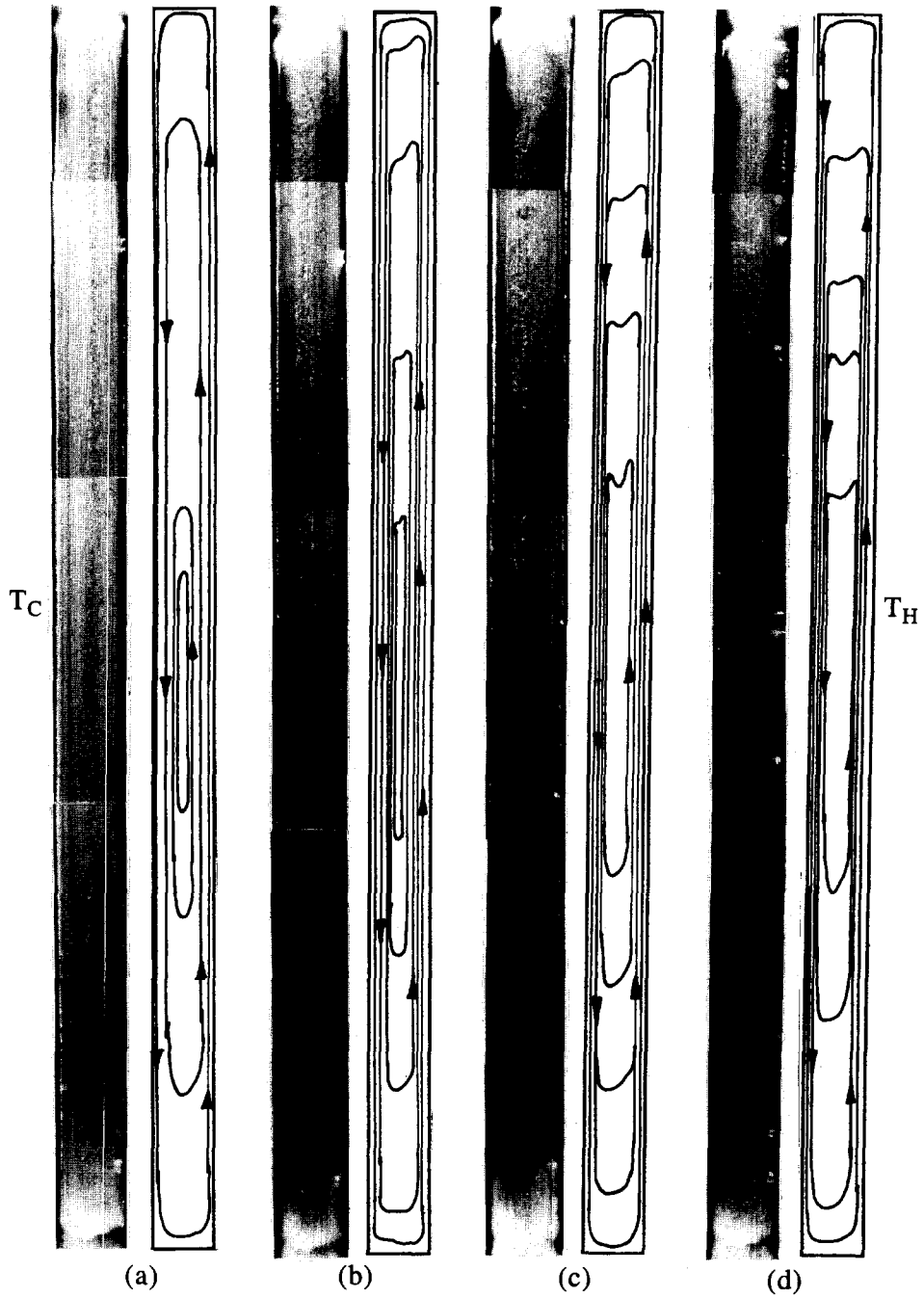

Fig. 4. Streak photograph in vertical central plane ($z = 0.5W$) in water: (a) $Ra = 1.58 \times 10^9$; (b) $Ra = 4.75 \times 10^9$; (c) $Ra = 8 \times 10^9$; (d) $Ra = 1.48 \times 10^{10}$.

situation becomes less evident far away from the $y = 0.5H$ (e.g. $y = 0.7H$ and $y = 0.3H$). Velocity profiles of the hot walls at different heights of the enclosure suggest the growth of a boundary-layer. The vertical velocity boundary-layer thickness increases as y/H gets larger. Again, the lack of symmetry is mainly attributed to fluid property variations with temperature. In addition to the previous qualitative comparison, experimentally measured vertical velocities for $Ra \cong 1.48 \times 10^{10}$ are also compared in Fig. 6(a) with those measured by Morrison and Tran [13] at $y = 0.5H$.

The presence of core horizontal stratification (conduction dominated) and its effect on the velocity profiles is more pronounced at high Rayleigh numbers (see Fig. 4 for details). Consider, for instance, the upward flow on the hot wall—hot fluid flowing in the boundary-layer finds itself in an environment (core) having a higher temperature. The temperature of the outer portion of the boundary-layer 'lags' behind that

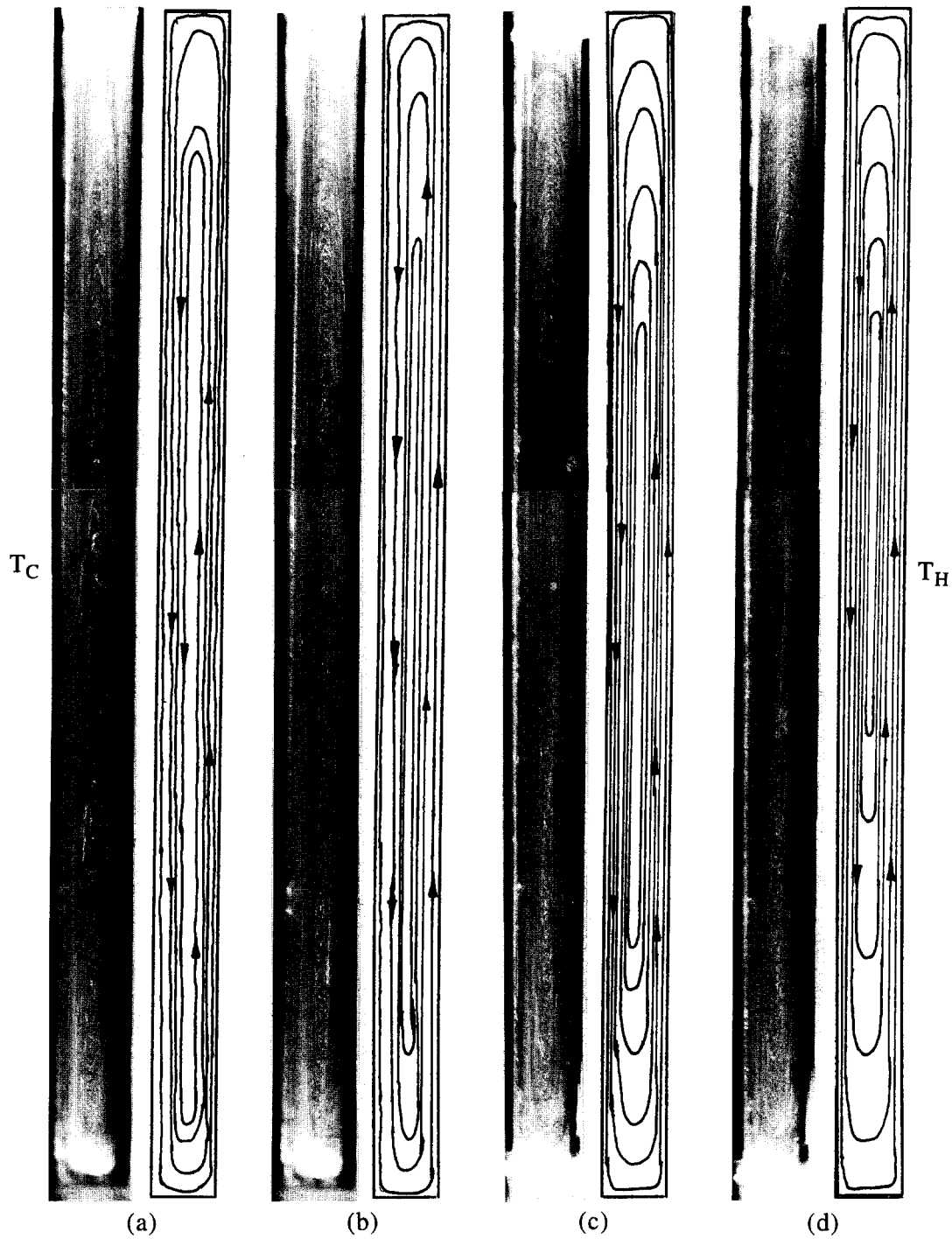

Fig. 5. Streak photograph in vertical central plane ($z = 0.5W$) in silicone oil: (a) $Ra = 1.54 \times 10^8$; (b) $Ra = 3.08 \times 10^8$; (c) $Ra = 6.48 \times 10^8$; (d) $Ra = 1 \times 10^9$.

of the stratified core. This results in the present v^+ distribution in the outer portion of the boundary layer as shown in Fig. 6(a).

Similar statements hold for the case of the downward boundary-layer flow at the cold wall. The three dimensional structure of the flow in the enclosure inferred from the vertical velocity measurements was studied by LDV to measure the horizontal velocity component parallel to the vertical heat transfer wall (w^+) at $y = 0.9H$ and $x = 0.5L$. The normalized velocity for the three components calculated were based on the u_{max}, v_{max} and w_{max} values listed in Table 3 at different *Ra*s.

In the central zone ($z^+ = 0.5W$) of the enclosure w^+ was found to be relatively strong, as shown in Fig. 6(b) at different *Ra*s. Moreover, measurements

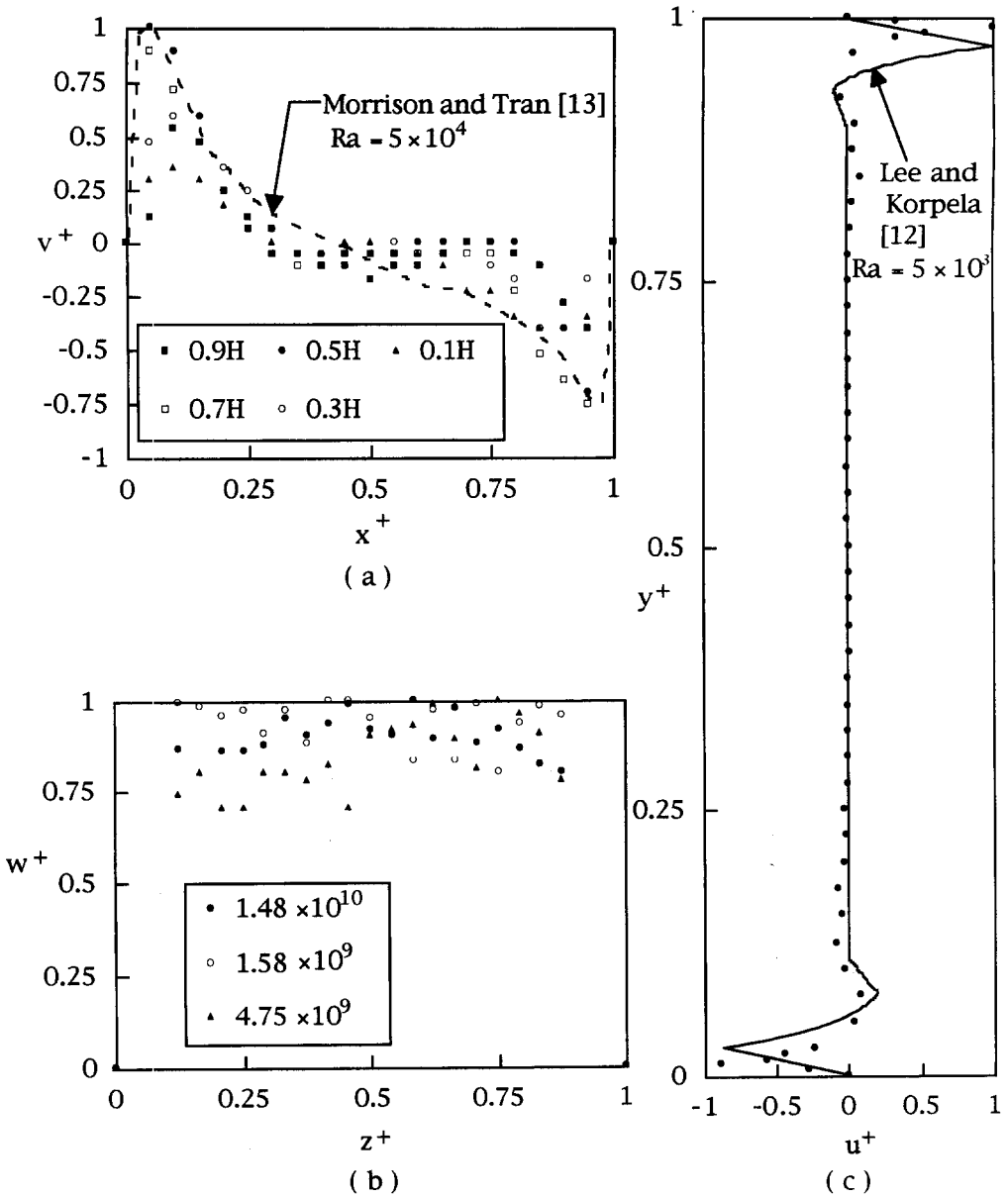

Fig. 6. Velocity profiles in water under various Rayleigh numbers: (a) y-component velocity at different elevations for $Ra = 1.48 \times 10^{10}$, $z = 0.5W$; (b) z = component velocity for $y = 0.9H$, $x = 0.5L$; (c) x-component velocity for $Ra = 1.48 \times 10^{10}$, $x = 0.5L$ and $z = 0.5W$.

at positions in the central plane, but off the horizontal central plane ($y = 0.9H$), also indicated a considerably large horizontal velocity, but had a different value at different measurement points, which also suggests the horizontal velocity is z^+ dependent. Owing to the uncertainty of $\pm 1\%$, we would rather believe a significant variation than a scatter. These profiles indicate that after passing over the top boundary of the enclosure the flow develops a horizontal velocity component directed towards the end walls. Figure 6(c)

Table 3. Normalized velocities in u, v and w components under different Ra

	$Ra = 1.58 \times 10^9$	$Ra = 4.75 \times 10^9$	$Ra = 8 \times 10^9$	$Ra = 1.48 \times 10^{10}$
u_{max}	—	—	—	0.656 cm s^{-1}
v_{max}	1.43 cm s^{-1}	1.75 cm s^{-1}	1.86 cm s^{-1}	2.15 cm s^{-1}
w_{max}	0.119 cm s^{-1}	0.144 cm s^{-1}	—	0.169 cm s^{-1}

—: stands for data not available.

shows the horizontal velocity distributions. The core shear profile is independent of x^+ and the layers near the horizontal walls are not small.

Generally speaking, the results shown in Fig. 6(c) agree with those reported by Lee and Korpela [12]. The experiments indicate the existence of a region ($0.03 \leqslant y \leqslant 0.97$) with very low velocity in which a weak secondary motion (traveling-wave type) occurs. This region would extend as Ra increases, which agrees with results calculated by Fusegi *et al.* [14].

To get further information, velocity profiles on hot walls in Fig. 6(a) were redrawn and enlarged at different heights of the enclosure and are thus presented in Fig. 7. It is observed that the peak velocity shifts a little bit away from the wall and its magnitude appears to increase for the first three measurement points, reaching a maximum at $y = 0.5H$ and then decreases as the flow proceeds downstream. This suggests the growth of a boundary-layer. When it approaches $x^+ = 0.25$, v^+ approaches zero. The asymmetry is again found in the vertical direction as one would expect. The maximum peak velocity occurred at $y = 0.5H$.

Also shown in Fig. 7 are 2-D numerical results from Ozoe *et al.* [15] at $y = 0.3$–$0.5H$ for comparison. The profiles are similar in shape but the experimental peak value at $y = 0.5H$ seems a little bit higher due to different Ras. This effect is also clearly noted in Fig. 7(b)–(d). Generally, v^+ increases as Ra increases. As the Rayleigh number is increased, the thickness of the velocity and temperature boundary-layer decreases (which will be shown later). Among the three velocity components, v has the largest velocity followed by u and w at a particular given position in the enclosure under the same conditions (see u_{max}, v_{max} and w_{max} in Table 3 for details).

4.3. *Temperature distribution*

The vertical temperature distribution in the core of the enclosure was obtained because the stable thermal stratification significantly influences the boundary-layer flows. In Figs. 8–9 the dimensionless core temperature ($T - T_C/T_H - T_C$) at five vertical positions are $z/W = 0.5$ and $x/L = 0.5$ for different Rayleigh numbers is presented for water and silicone oil, respectively.

At $z = 0.5W$, in Fig. 8, convection dominates in the central region and becomes more evident as Rayleigh number increases. The temperature field is linearly stratified in the vertical direction and practically independent of the distance from the wall except for thin regions near the hot wall and cold wall where sharp thermal boundary-layers exist.

Figure 8 reveals that the heat is mainly transported from the hot wall to the cold wall by tangential convection. Furthermore, temperature inversions were observed in the central plane ($0.5 \leqslant x/L \leqslant 0.75$) as $Ra \geqslant 4.75 \times 10^9$ which indicates a manifestation of the flow immediately adjacent to the vertical wall, which is so strong that it produces a high rate of tangential convection of heat along the surface of the hot wall relative to the vertical transport of heat from the surface of the hot wall across to the cold wall. A similar trend occurred in the study of Elder [10] in which he found numerous secondary vortices occurring in the core at high Rayleigh numbers. A flow field under such circumstances, with a core of uniform temperature along the horizontal direction is referred to as 'boundary-layer regime'.

However, the situation for silicone oil shows a different trend, in which a linear temperature distribution occurs across the core of the enclosure, indicating that the heat from the hot wall to the cold wall is transported by conduction through the major portion of the core and by convection at the bottom of the hot wall and the top of the cold wall. This is also verified by previous velocity measurements as shown in Fig. 6(a). At $x/L = 0.5$, in Fig. 8, there is a strong suggestion that the temperature seems independent of the z^+-direction at all Ras and temperature stratification is still found. This indicates that the present temperature distribution is 2-D which is different from the previous measurement for flow structure. A similar situation also occurred for silicone oil as shown in the lower part of Fig. 9.

4.4. *Nusselt number correlation*

For each steady state the net heat transfer rate through the enclosure was calculated and is reported in terms of a Nusselt number and Rayleigh number correlation based on equations (1) and (2). The Nusselt number as a function of Ra is presented in Fig. 10. The current results permit the identification of only two regions of heat transfer—the laminar and turbulent regimes.

Through multiple regression analysis, it is found that

$$Nu = 0.224 Ra^{0.257} Pr^{0.056} \quad \text{(for the laminar regime)}$$

$$Ra < 3 \times 10^9 \quad (3)$$

and

$$Nu = 0.059 Ra^{0.315} Pr^{0.056} \quad (4)$$

$$\text{(for the turbulent regime)} Ra \geqslant 3 \times 10^9$$

within $\pm 5\%$ of the experimental data. Table 4 summarizes the previous relevant work for both numerical and experimental studies in comparison with the present work. The present Nu data correlate well with a nearly 1/4 power of Ra, as predicted from the laminar boundary-layer theory. The bifurcation point is located at $Ra \cong 3.0 \times 10^9$ which is much greater than usual (e.g. $Ra = 1.4 \times 10^7$, see Hsieh and Wang, [8]) owing to the present narrow geometry.

The bifurcation point can also be observed from the flow visualization, this agrees with the findings of Macgregor and Emery [16] and Seki *et al.* [17]. It appears that the nearness of the two vertical walls tends to dampen or to inhibit the growth of oscil-

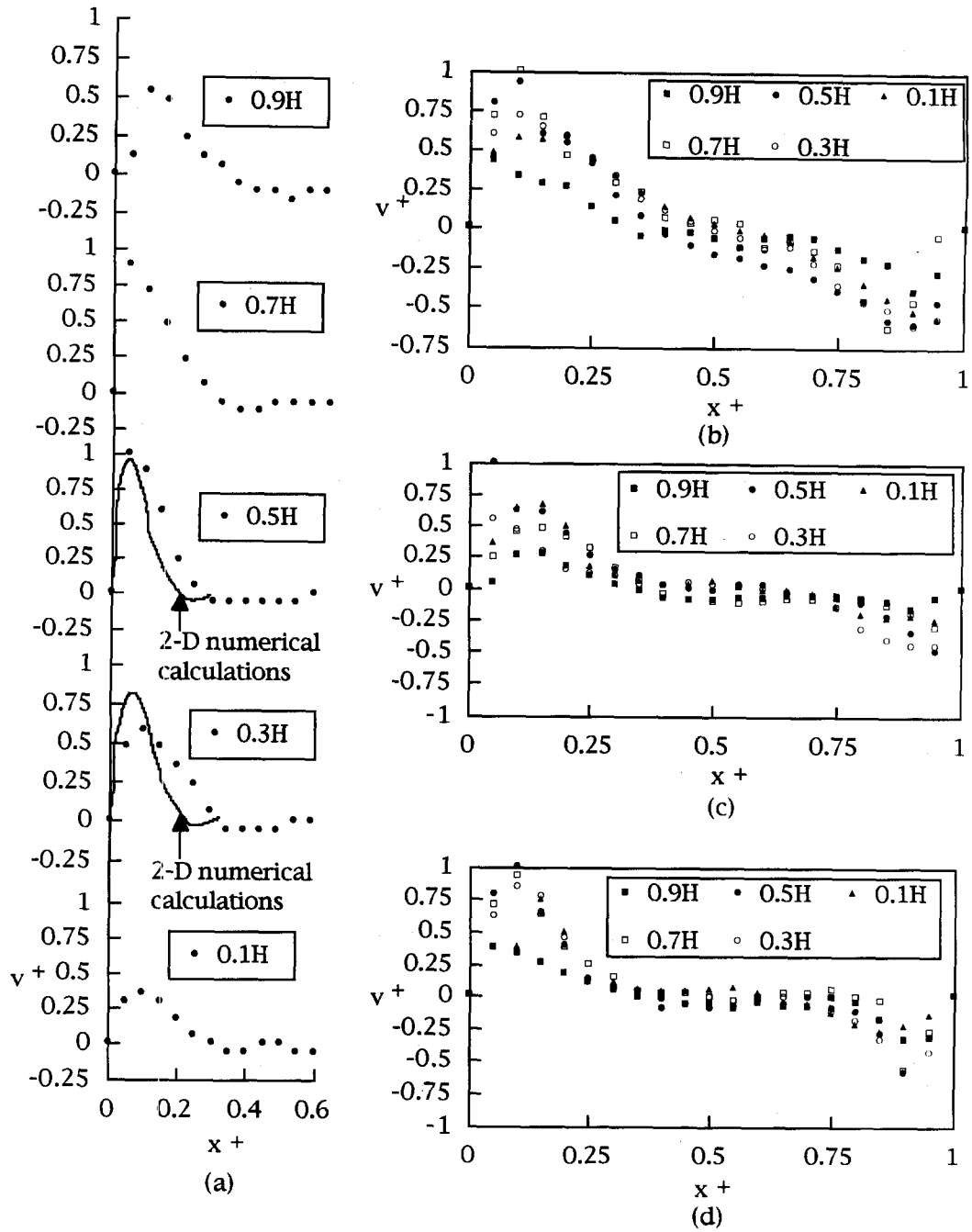

Fig. 7. (a) Comparison of the vertical velocity near the heated wall: (—)$Ra = 10^9$, Ozoe *et al.* [15]; (●) $Ra = 1.48 \times 10^{10}$ present study vertical velocity profiles at different elevations for (b) $Ra = 1.58 \times 10^9$, (c) $Ra = 4.75 \times 10^9$, (d) $Ra = 8 \times 10^9$.

lations which results in a delay in the onset of turbulence. Exact reasons are still not well understood at this stage. A systematic further study of the effect of the aspect ratio upon the transition from laminar to turbulent flow is essentially needed. This observation further shows that the heat transfer mechanism is laminar convection when close vertical walls surround the core regime at $Ra < 3.0 \times 10^9$. Furthermore, it was visually observed that with silicone oil inside the enclosure the boundary-layer showed that the laminar boundary-layer exists along the walls.

When $Ra \geqslant 3 \times 10^9$, based on flow visualization, it is found that a substantial portion of the wall boundary-layer becomes turbulent which results in an $Ra^{1/3}$ dependence. Previous relevant studies with water inside an enclosure were also shown in Fig. 10 for comparison. Furthermore, Table 4 summarizes the previous relevant work for both numerical and exper-

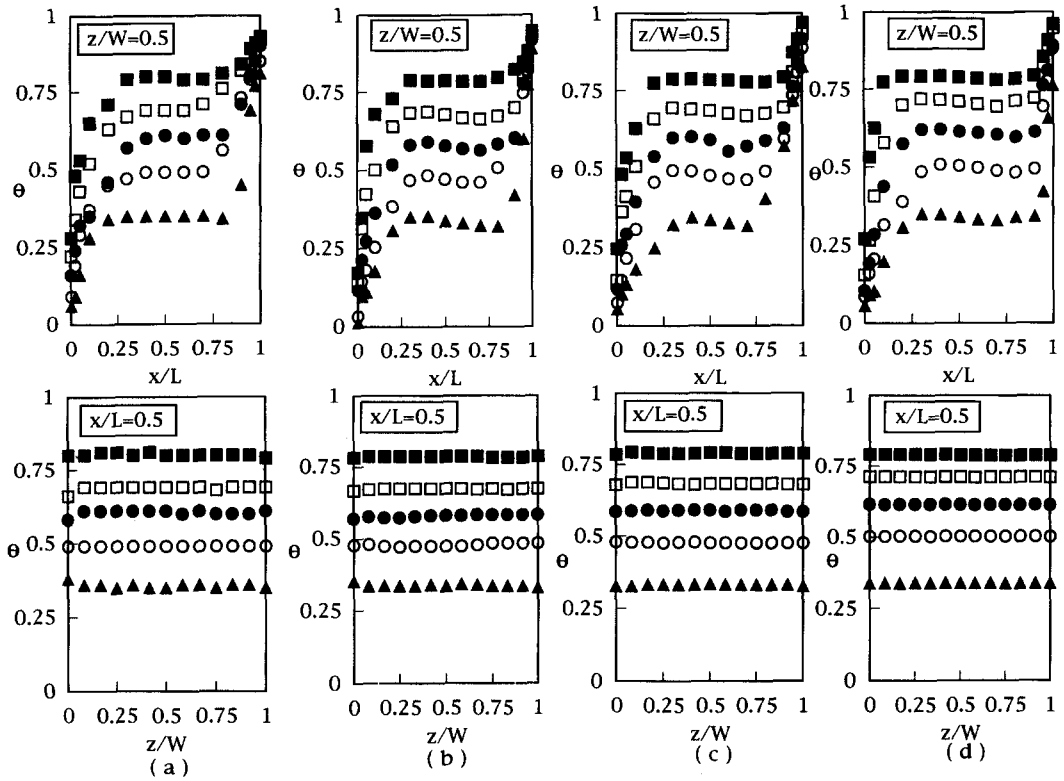

Fig. 8. Temperature distributions at different elevations: (■) $y = 0.9H$; (□) $y = 0.7H$; (●) $y = 0.5H$; (○) $y = 0.3H$; (▲) $y = 0.1H$, for different Ra; (a) $Ra = 1.58 \times 10^9$; (b) $Ra = 4.75 \times 10^9$; (c) $Ra\ 8 \times 10^9$; (d) $Ra = 1.48 \times 10^{10}$ for water.

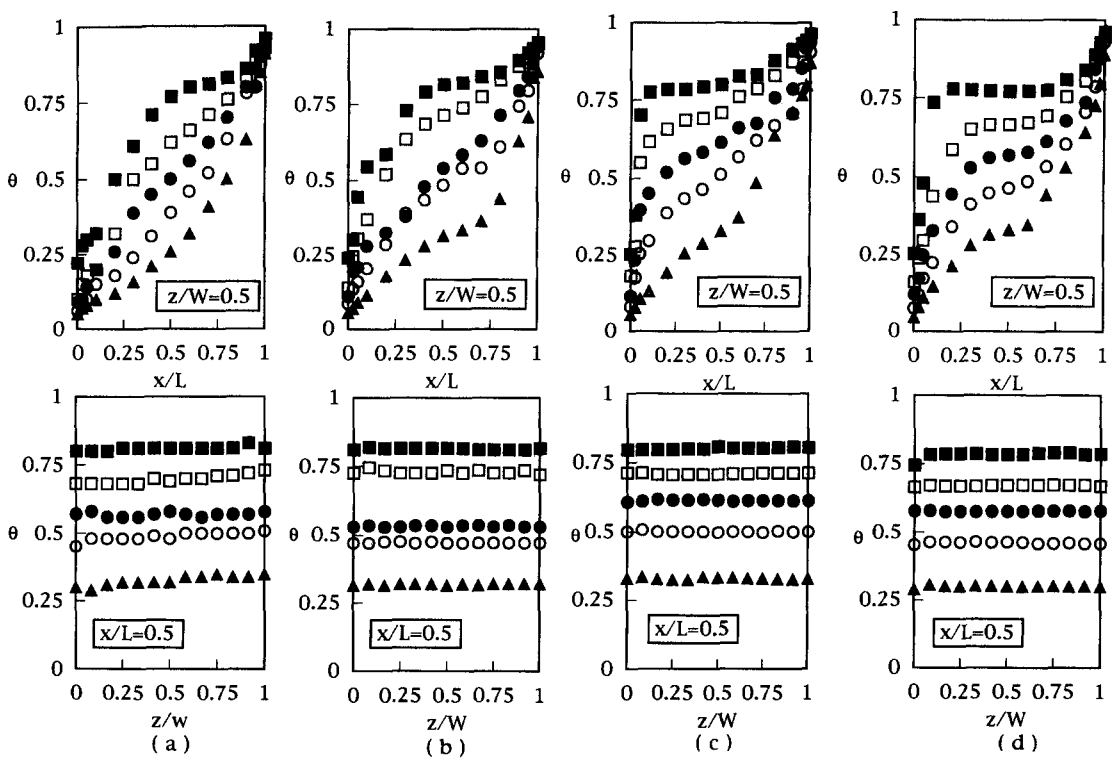

Fig. 9. Temperature distributions at different elevations: (■) $y = 0.9H$; (□) $y = 0.7H$; (●) $y = 0.5H$; (○) $y = 0.3H$; (▲) $y = 0.1H$ for different Ra; (a) $Ra = 1.54 \times 10^8$; (b) $Ra = 3.08 \times 10^8$; (c) $Ra = 6.48 \times 10^8$; (d) $Ra = 1 \times 10^9$ for silicone oil.

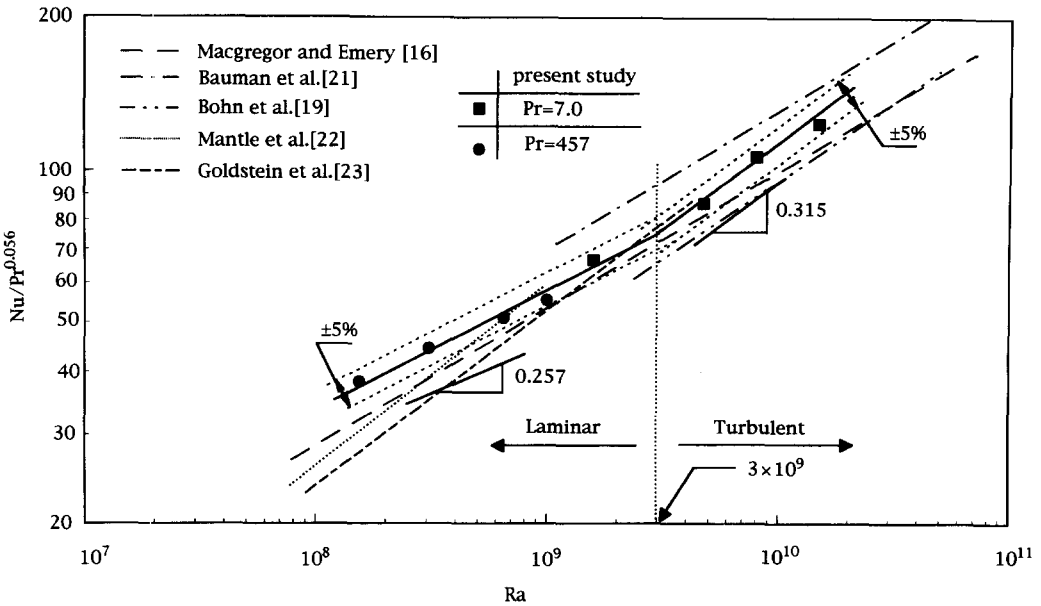

Fig. 10. *Nu* vs *Ra*.

imental studies, with the present work. The large exponent of *Ra* indicates a strong contribution by convection to the overall heat transfer.

Table 5 relists Table 4 results without inclusion of the aspect ratio and Prandtl number effect, with the addition of results from Bohn *et al.* [19] for a 3-D cubic enclosure. The present results seem to have a higher *Nu* value in both laminar and turbulent regimes—this can also be seen in Fig. 10. But, nevertheless, the Rayleigh number dependence is in good agreement with those listed in Table 5.

5. CONCLUSION

The paper presents an experimental study for buoyancy-induced natural convection at high Rayleigh numbers (1.58×10^8–1.48×10^{10}) inside a rectangular enclosure with aspect ratios $H/L = 20$ and $W/L = 6$ wherein the right vertical wall was heated and the left vertical wall was cooled. The remaining four walls were adiabatic except when flow visualization was performed.

Flow visualization and 3-D LDV as well as temperature measurements were conducted for water and silicone oil as the working mediums. The most significant features of the study are:

(1) Flow visualization for the present study ($A_H = 20$) shows that a unicellular motion, with the instability of a traveling-wave type, exists up to $Ra = 1.48 \times 10^{10}$.

(2) Flow structure was examined through 3-D LDV measurements. Three dimensional effects (w^+ is dependent on z^+ direction) were obviously found in the present geometry while temperature measurements show a 2-D behavior (θ is independent of z^+ direction).

Table 4. Existing data for experimental and numerical studies in rectangular square enclosures

Relevant study	Correlations		Working medium	Geometry enclosure
	Laminar	Turbulent		
[17]	$Nu = 0.36\mathrm{Ra}^{0.25}\mathrm{Pr}^{0.051}\mathrm{A_H}^{-0.11}$ $10^7 < Ra < 10^9$ $6 < A_H < 30$	$Nu = 0.096Ra^{0.3}Pr^{0.051}$ $10^{10} < Ra < 10^{11}$ $6 < A_H < 30$	Transformer Oil Water Glycerin	2-D
[16]	$Nu = 0.42Ra^{0.25}Pr^{0.012}A_H^{-0.3}$ $10^4 \leqslant Ra \leqslant 10^6$ $10 < A_H < 40$	$Nu = 0.046Ra^{1/3}$ $10^7 \leqslant Ra \leqslant 10^{12}$ $1 < A_H < 40$	Glycerin Castor oil Water Ethyl alcohol	2-D
[18]	—	$Nu = 0.049Ra^{1/3}Pr^{0.074}$ $5 \times 10^4 < Ra < 2.5 \times 10^8$ $4 \leqslant A_H \leqslant 16$	Water Silicone oil Mercury	2-D
Present study	$Nu = 0.224Ra^{0.257}Pr^{0.056}$ $1.54 \times 10^8 \leqslant Ra \leqslant 1.58 \times 10^9$ $A_H = 20$	$Nu = 0.059Ra^{0.315}Pr^{0.056}$ $1.58 \times 10^9 \leqslant Ra \leqslant 1.48 \times 10^{10}$ $A_H = 20$	Water Silicone oil	3-D

—: stands for data not available.

Table 5. Correlation for the present results and comparison with those of the relevant studies (aspect ratio and Prandtl number are not included)

Relevant study	Correlations		Working medium	Geometry enclosure
	Laminar	Turbulent		
[20]	$Nu = 0.27Ra^{0.25}$ $10^7 < Ra < 10^9$ $6 < A_H < 30$	$Nu = 0.1Ra^{0.3}$ $10^{10} < Ra < 10^{11}$ $6 < A_H < 30$	Transformer Oil Water Glycerin	2-D
[16]	$Nu = 0.2Ra^{0.25}$ $10^4 \leqslant Ra \leqslant 10^6$ $1 < A_H < 40$	$Nu = 0.046Ra^{1/3}$ $10^7 \leqslant Ra \leqslant 10^{12}$ $1 < A_H < 40$	Glycerin Castor oil Water Ethyl alcohol	2-D
[18]	—	$Nu = 0.054Ra^{1/3}$ $5 \times 10^4 < Ra < 2.5 \times 10^8$ $4 \leqslant A_H \leqslant 16$	Water Silicon oil Mercury	2-D
[19]	$Nu = 0.31Ra^{0.25}$ $0.3 \leqslant Ra \leqslant 10^{10}$ $A_H = 1$	—	Water	3-D
Present study	$Nu = 0.46Ra^{0.235}$ $1.54 \times 10^8 \leqslant Ra \leqslant 1.58 \times 10^9$ $A_H = 20$	$Nu = 0.076Ra^{0.31}$ $4.75 \times 10^9 \leqslant Ra \leqslant 1.48 \times 10^{10}$ $A_H = 20$	Water Silicon oil	3-D

—: stands for data not available.

(3) It was observed that the transition of a boundary-layer regime occurred at $Ra = 3 \times 10^9$ to bifurcate the laminar and turbulent flow. An obvious delay in the onset of turbulence occurs in this narrow, tall 3-D enclosure.

(4) The 3-D effect was found based on flow velocity measurements and flow visualization.

REFERENCES

1. Ostrach, S., Natural convection in enclosures. *Advances in Heat Transfer*, 1972, **8,** 161–227.
2. Ostrach, S., Natural convection in enclosures. *ASME Journal of Heat Transfer*, 1988, **110,** 1175–1190.
3. Bejan, A., *Convection Heat Transfer*. Wiley, New York, 1984, pp. 159–201.
4. Hiller, W. J., Koch, S. and Kowalewski, T. A., Three-dimensional structures in laminar natural convection in a cubic enclosure. *Experiments in Thermal Fluid Science*, 1989, **2,** 34–44.
5. Hoogendoorn, C. J., Natural convection in enclosures. *Eighth International Heat Transfer Conferences*, 1986, **1,** 111–120.
6. Ozoe, H., Ohmuro, M., Mouri, A., Mishima, S., Sayama, H. and Churchill, S. W., Laser-Doppler measurements of the velocity along a heated vertical wall of a rectangular enclosure. *ASME Journal of Heat Transfer*, 1983, **105,** 782–788.
7. Lankhorst, A. M., Angirasa, D. and Hoogendoorn, C. J., LDV measurements of buoyancy-induced flows in an enclosure at high Rayleigh numbers. *Experiments in Thermal Fluid Science*, 1993, **6,** 74–79.
8. Hsieh, S. S. and Wang, C. Y. Experimental study of three-dimensional natural convection in enclosures with different working fluids. *International Journal of Heat and Mass Transfer*, 1994, **37,** 2687–2698.
9. Kline, S. J. and McClintock, F. A., Describing uncertainties in single sample experiments. *Mechanical Engineering*, 1953, **75,** 3–8.
10. Elder, J. W., Turbulent free convection in a vertical slot. *Journal of Fluid Mechanics*, 1965, **23,** 99–111.
11. Bergholz, R. F., Instability of steady natural convection in a vertical fluid layer. *Journal of Fluid Mechanics*, 1978, **84,** 743–768.
12. Lee, Y. and Korpela, S. A., Multicellular natural convection in a vertical slot. *Journal of Fluid Mechanics*, 1983, **126,** 91–121.
13. Morrison, G. L. and Ran, V. Q., Laminar flow structure in vertical free convection cavities. *International Journal of Heat and Mass Transfer*, 1977, **21,** 203–213.
14. Fusegi, T., Hyun, J. M., Kuwahara, K. and Farouk, B., A numerical study of three-dimensional natural convection in a differentially heated cubical enclosure. *International Journal of Heat and Mass Transfer*, 1991, **34,** 1543–1557.
15. Ozoe, H., Mouri, A., Ohmuro, M., Churchill, S. W. and Lior, N., Numerical calculations of laminar and turbulent natural convection in water in rectangular channels heated and cooled isothermally on the opposing vertical walls. *International Journal of Heat and Mass Transfer*, 1985, **28,** 125–138.
16. Macgregor, R. K. and Emery, A. F., Free convection through vertical plane layers—moderate and high Prandtl number fluids. *ASME Journal of Heat Transfer*, 1969, **91,** 391–403.
17. Seki, N., Fukusako, S. and Inaba, H., Visual observation of natural convection flow in a narrow vertical cavity. *Journal of Fluid Mechanics*, 1978, **84,** 695–704.
18. Dropkin, D. and Somerscales, E., Heat transfer by natural convection in liquids confined by two parallel plates which are inclined at various angles with respect to the horizontal. *ASME Journal of Heat Transfer*, 1965, **87,** 77–86.
19. Bohn, M. S., Kirkpatrick, A. T. and Olson, D. A., Experimental study of three-dimensional natural convection high-Rayleigh number. *ASME Journal of Heat Transfer*, 1984, **106,** 339–345.
20. Nobuhino, S. and Fukusako, S., Visual observation of natural convection flow in a narrow vertical cavity. *Journal of Fluid Mechanics*, 1978, **84,** 695–704.